The cell cycle oscillator and spindle length set the speed of chromosome separation in *Drosophila* embryos

Yitong Xu[1], Anna Chao[1], Melissa Rinaldin[2,3,4], Alison Kickuth[2,3,4], Jan Brugués[2,3,4], Stefano Di Talia[1,*]

[1] Department of Cell Biology, Duke University Medical Center, Durham NC 27705, USA

[2] Cluster of Excellence Physics of Life, TU Dresden, Dresden, 01307 Germany

[3] Max Planck Institute of Molecular Cell Biology and Genetics, Dresden, 01307 Germany

[4] Center of Systems Biology, Dresden, 01307 Germany

*correspondence to: stefano.ditalia@duke.edu

Summary

Anaphase is tightly controlled in space and time to ensure proper separation of chromosomes. The mitotic spindle, the self-organized microtubule structure driving chromosome segregation, scales in size with the available cytoplasm. Yet, the relationship between spindle size and chromosome movement remains poorly understood. Here, we address how the movement of chromosomes changes during the cleavage divisions of the *Drosophila* blastoderm. We show that the speed of chromosome separation gradually decreases during the 4 nuclear divisions of the blastoderm. This reduction in speed is accompanied by a similar reduction in the length of the spindle, thus ensuring that these two quantities are tightly linked. Using a combination of genetic and quantitative imaging approaches, we find that two processes contribute to controlling the speed at which chromosomes move at mitotic exit: the activity of molecular motors important for microtubule depolymerization and the cell cycle oscillator. Specifically, we found that the levels of Klp10A, Klp67A, and Klp59C, three kinesin-like proteins important for

microtubule depolymerization, contribute to setting the speed of chromosome separation. This observation is supported by quantification of microtubule dynamics indicating that poleward flux rate scales with the length of the spindle. Perturbations of the cell cycle oscillator using heterozygous mutants of mitotic kinases and phosphatases revealed that the duration of anaphase increases during the blastoderm cycles and is the major regulator of chromosome velocity. Thus, our work suggests a potential link between the biochemical rate of mitotic exit and the forces exerted by the spindle. Collectively, we propose that the cell cycle oscillator and spindle length set the speed of chromosome separation in anaphase.

Results

In *Drosophila* embryos, early development is characterized by rapid and synchronous syncytial nuclear divisions [1, 2]. At the blastoderm stage, multiple nuclear divisions occur simultaneously on the surface of the embryo. These mitoses drive a reduction in the spacing among nuclei, which, in turn, results in smaller mitotic spindles. To elucidate the relationship between spindle size and chromosome separation, we used confocal live imaging to study anaphase in early fly embryos.

Using embryos maternally expressing histone tagged with GFP (His2Av-GFP) and a microtubule fluorescent reporter (mCherry fused to the Tau microtubule-binding domain) [3], we imaged nuclear divisions and microtubule dynamics from cycle 10 to cycle 13 (Fig 1A-B). As the nuclear cycles progressed, the number of nuclei at the surface of the embryo increased exponentially, while the spacing among nuclei proportionally reduces. This means chromosomes in an early cycle (e.g. Cycle 10) possess larger room for separation than chromosomes in a later cycle (e.g. Cycle 13). Likewise, mitotic spindles were proportionally smaller as the embryo approached later cycles (Fig 1A). We used the histone signal to segment chromosomes and tracked their segregation in individual nuclei [4]. To quantify the velocity of chromosome separation, we measured the speed at which the leading edges of segregating sister chromatids

58 move apart from each other (Fig 1C, S1). These measurements revealed a compelling
59 finding: the speed at which chromosomes separate during anaphase exhibits a scaling
60 relationship with spindle length (estimated here as the maximum distance of
61 chromosome separation, see Fig S1) (Fig 1H). This scaling ensures that chromosome
62 separation has a similar duration- approximately 70 seconds- in all nuclear cycles (Fig
63 1C). Moreover, the dynamics of the distance between sister chromosomes can be
64 collapsed for all cycles when normalized by total distance that is covered in each cycle
65 (Fig 1D), suggesting that the dynamics are essentially indistinguishable when rescaled
66 for spindle length. Additionally, we found that both the movement of the chromosome
67 towards the spindle pole (Anaphase A) and the movement of spindle poles away from
68 each other (Anaphase B) demonstrated scaling with spindle length (Fig 1E-G).
69 Quantitative comparison of the chromosomes movements due to these two processes
70 confirmed that, as expected, chromosome separation is dominated by Anaphase A in
71 fly embryos [5, 6] (Fig F-G, S1). Collectively, these observations point to an interesting
72 correlation between the speed of chromosome separation and the length of the mitotic
73 spindle.

74 To elucidate the connection between spindle length and chromosome separation speed,
75 we first considered the potential role of microtubule dynamics. To this end, we
76 conducted a series of experiments to quantify different parameters of spindle
77 microtubule dynamics. First, we investigated microtubule density along the pole-to-
78 pole axis during mitosis. As chromosomes separate and spindles elongate, the spatial
79 distribution of microtubules remains largely unchanged, exhibiting no discernable
80 correlation with chromosome (and kinetochore microtubules) position, until the spindle
81 disassembles (Fig 2A-B). Thus, in early anaphase, kinetochore microtubules likely
82 represent a small fraction of spindle microtubules. The decrease in spindle length from
83 cycle 10 to cycle 13 is accompanied by a decrease in microtubule density (Fig 2C-D).
84 Secondly, we performed tracking of microtubule plus-ends and quantified the rate of
85 microtubule polymerization, using embryos expressing microtubule plus-end binding
86 protein EB1-GFP [7-10]. Our analysis revealed that the polymerization velocity of

87 microtubules has a significant, although slight, dependency on spindle length, as
88 polymerization velocity increases about 20% when spindle length doubles (Fig 2E-F).
89 A similar positive correlation between spindle length and microtubule polymerization
90 velocity has been observed in zebrafish, *C. elegans* and sea urchin [8, 11]. However,
91 the extent of this correlation quantitatively changes in these organisms: a strong
92 dependency of polymerization speed on spindle length is observed in sea urchin and *C.*
93 *elegans*, while a small dependency is observed in zebrafish, similar to the one seen here
94 for *Drosophila*.

95 This observation argues that microtubule polymerization contributes partially to the
96 modulation of spindle length in the *Drosophila* blastoderm. Finally, we employed
97 femto-second laser ablation to sever microtubules within the metaphase spindle,
98 inducing microtubule depolymerization [12, 13]. A consistent rate of depolymerization
99 of approximately 0.6μm/s (35μm/min) was observed, regardless of the specific cell
100 cycle stage or spindle length, which demonstrated that the rate of depolymerization of
101 unstable microtubules does not change during cycle 10 to 13 (Fig 2G-H). This
102 observation and the fact that the measured value is consistent with values observed in
103 other systems argue that this constant rate of depolymerization is set by the intrinsic
104 properties of microtubule catastrophe dynamics. These observations on microtubule
105 dynamics are similar to previous findings in zebrafish [8], suggesting a conserved
106 mechanism for the scaling of spindle size during *Drosophila* blastoderm divisions.
107 However, they do not explain the relationship between spindle length and chromosome
108 speed.

109 Poleward movement of chromosomes (Anaphase A) is achieved by the shortening of
110 kinetochore-associated microtubules, while the separation of opposite spindle poles
111 (Anaphase B) is driven by the sliding of interpolar microtubules. Both processes
112 involve forces generated on the microtubules by motor proteins. Thus, we turned our
113 attention to the molecular motors involved in those processes and more specifically
114 motors that play a role in shortening kinetochore-associated microtubules, given the

115 dominant contribution of Anaphase A to chromosome separation. To this end, we first
116 analyzed microtubule poleward flux, that is the continuous movement of tubulin
117 subunits towards the centrosome [14-16]. We note that for kinetochore-associated
118 microtubules during anaphase, poleward flux is driven by microtubule
119 depolymerization at both the centrosome (minus end) and at the kinetochore (plus end),
120 due to the activity of specific motors [17, 18]. For polar microtubules, poleward flux
121 could be due to either depolymerization at the centrosome or microtubule sliding. To
122 estimate poleward flux in the fly embryos, we employed a transgenic line in which
123 tubulin is tagged with a photo-convertible tdEOS fluorescent protein that can be
124 converted from green to red upon UV illumination [19]. To describe poleward fluxes
125 in anaphase, we monitored spindle morphology under the confocal microscope in living
126 embryos [20]. As nuclei approached anaphase onset, we photo-converted a small region
127 of microtubules near the mid-spindle and tracked it for 20-30 seconds during early
128 anaphase (Fig 3A). The calculated poleward flux rates were comparable to the speed of
129 chromosome movement at anaphase onset and similar to previously reported values
130 [16]. The flux rate showed a clear dependency on spindle length, suggesting that it
131 might be implicated in setting the speed of chromosome movement in anaphase (Fig
132 3B).

133 To strengthen this point, we analyzed whether motors implicated in Anaphase A and B
134 movement, namely Klp10A, Klp67A, Klp59C and Klp61F, are rate-limiting for
135 chromosome movements (Fig 3C). We used heterozygous mutants to lower their
136 activity without fully abrogating it. We analyzed chromosome velocity and spindle
137 length in these mutants and found that they retain a strong relationship between
138 chromosome speed and spindle length (Fig 3D). Consistent with the dominant role of
139 Anaphase A in controlling chromosome movements, we found that perturbing the level
140 of Klp61F, the microtubule sliding motor driving Anaphase B, has no significant effect
141 on chromosome speed (Fig S2). Notably, all heterozygous mutants of microtubule
142 depolymerase display a significant reduction in the speed of chromosome separation
143 for a given spindle length (Fig 3E). Similar effects were observed for motors acting at

144 the centrosome (Klp10A) and at the kinetochore (Klp67A and Klp59C), suggesting that
145 both processes contribute to chromosome movements in comparable manner (Fig 3E).
146 Klp10A also localizes to the kinetochore, but its activity at the kinetochore is believed
147 to be weaker than at the centrosome [18]. Assuming that the movement of
148 chromosomes is dependent on the balance of polymerization and depolymerization rate
149 of kinetochore microtubules, we can estimate the speed of chromosome as:

150 $$v_{chr} \propto k_{dep}^{kin} + k_{dep}^{cen} - k_{p}^{kin}$$

151 and the speed of poleward flux as:

152 $$v_{pf} \propto k_{dep}^{cen}$$

153 where k_{dep} indicates the rates of depolymerization, k_p designates the rate of
154 polymerization, k^{kin} indicates the rates at the kinetochore and k^{cen} indicates the rates
155 at the centrosome. Since we found that:

156 $$v_{pf} \approx v_{chr}$$

157 we conclude that the rate of polymerization and depolymerization at the kinetochore
158 must almost balance each other out, that is:

159 $$k_{dep}^{kin} \approx k_{p}^{kin}$$

160 This relationship would suggest that the rate of depolymerization at the kinetochore
161 decreases from cycle 10 to 13, as we previously found that microtubule polymerization
162 shows a positive dependency on spindle length (Fig 2F). These results indicate that the
163 scaling of chromosome movement with spindle length might be the result of changes
164 in the rate of microtubule polymerization and depolymerization. Moreover, our genetic
165 experiments implicate multiple motors in this process, thus suggesting that there might
166 be a global mechanism controlling the activity of molecular motors in anaphase.

167 A natural candidate for such regulation is the cell cycle oscillator, as the activity of the
168 motors must be controlled in space and time during the cell cycle. Specifically, we
169 hypothesized that the rate of phosphorylation and dephosphorylation of mitotic targets
170 involved in the function of the spindle might influence the speed of chromosome

171 separation. To test this hypothesis, we first investigated the relationship between
172 chromosome speed and spindle length in embryos heterozygous for several regulators
173 of the cell cycle (Fig 4C, E). Remarkably, we found that these mutations disrupted the
174 scaling relationship. Embryos with one less copy of Cyclin B displayed slightly slower
175 chromosome velocity. On the contrary, embryos with two extra copies of Cyclin B (*4x*
176 *cycB*) exhibited a faster chromosome separation speed. These observations suggest that
177 Cyclin B-Cdk1 plays a role in setting the speed of chromosome separation. We also
178 observed a reduction of chromosome velocity in *polo* (Plk1) and *twsP* (the B55
179 regulatory subunit of the PP2A phosphatase) heterozygous mutants. In *polo/+* embryos,
180 the nuclei migrating from the inner regions of the embryo reached the cortex at cycle 9
181 [21], that is one cycle earlier than in other genotypes, resulting in larger spindles at the
182 onset of the blastoderm stage. Moreover, some *polo/+* embryos failed to finish cycle
183 13, due to cell cycle defects and excessive crowding of the nuclei at the embryo cortex.
184 The *twsP/+* embryo displayed normal spindle length despite slower chromosome
185 speeds than wild-type. Finally, we found that *PP1-87B* and *PP1-96A* double
186 heterozygous mutant embryos had slightly larger spindles and speeds than wild-type
187 (similar to *4x cycB*) suggesting that Cdk1 and PP1 might have opposite impacts on
188 chromosome separation. Collectively, these results revealed a major role for the
189 components of the cell cycle oscillator in setting the speed of chromosome separation.

190 The cell cycle oscillator coordinates mitotic events in space and time (Fig 4C). In
191 mitosis, Cdk1 activity represses cytoplasmic microtubule polymerization by affecting
192 several microtubule-associated proteins (MAPs) and promotes spindle assembly and
193 chromosome alignment [22]. Polo kinase also controls several aspects of spindle and
194 centrosome behaviors [23-25]. The decrease of Cdk1 activity triggers the onset of
195 anaphase and the migration of chromosomes towards the poles. As Cdk1 and Polo
196 activities decrease in mitosis, mitotic substrates are dephosphorylated mainly by
197 PP1/PP2A phosphatases [26, 27]. Together the balance of mitotic kinases and
198 phosphatases controls all events at mitotic exit, including chromosome decondensation
199 and the reformation of the nuclear envelope. We operationally used nuclear envelope

200 reformation (NER) as a hallmark event to score the completion of anaphase [28, 29]
201 (Fig 4A-B). We hypothesize that the activity of cell cycle regulators set the rate of
202 completion of anaphase, which in turn contributes to setting the speed of chromosome
203 movement by influencing the activity of mitotic targets, such as molecular motors,
204 involved in spindle function. To measure anaphase rate in different cell cycles, we
205 defined anaphase duration from the initiation of chromosome segregation to nuclear
206 envelope reformation (Fig 4A-C). We used the intensity of nuclear-localized GFP to
207 estimate the time when nuclear envelope integrity was reestablished. Imaging this probe
208 together with histones showed that the reformation of nuclear envelope starts after the
209 segregation of chromosomes is completed (Fig S3). Our analysis showed that the
210 duration of anaphase gets progressively longer from nuclear cycle 10 to 13 (Fig 4D).
211 Moreover, we observed that the duration of anaphase is longer in the *cycB/+*, *polo/+*
212 and *twsP/+* heterozygous embryos (Fig 4F). Conversely, *4x cycB* embryos and PP1
213 heterozygous embryos showed shorter anaphase durations than wild-type. These
214 findings support the hypothesis that the activity of cell cycle regulators set the rate of
215 completion of anaphase.

216 Given the observed changes in anaphase duration, we tested whether the speed of
217 chromosome separation could be explained by these changes. In support of this idea,
218 we found a strong correlation between chromosome velocity and anaphase rate, and
219 most importantly, that such correlation holds essentially for all the mutants, so that all
220 the data can be collapsed on a single relationship (Fig 4F). This observation suggests
221 that the rate of progression through anaphase is a strong predictor, and most likely a
222 major regulator, of the speed of chromosome separation. Careful inspection of the data
223 showed that in regions where the anaphase rate overlapped between wild-type and
224 mutant embryos, the embryos with larger spindles tended to have slightly higher speeds.
225 This observation suggested that there is still some contribution to the speed of
226 chromosome movement from processes independent of anaphase duration. We
227 speculated that this residual contribution arises from differences in spindle length. Thus,
228 we used a simple linear model to test how much of the data can be captured by a linear

229 combination of anaphase duration and spindle length. After centering and
230 normalization of the two variables, we found that a linear combination of anaphase rate
231 and spindle length can predict chromosome speed with high accuracy in all the mutants
232 (R^2=0.84). This analysis suggests that anaphase rate accounts for 70% of the
233 dependency of chromosome velocity whereas residual contributions from spindle
234 length (or a closely correlated variable) might explain the remaining 30%. Collectively,
235 these results argue that the speed of chromosome separation is set by a combination of
236 biochemical cues from the cell cycle oscillator and mechanical cues from the mitotic
237 spindle.
238

239 **Discussion**

240 Anaphase is the culmination of mitosis, when duplicated chromosomes segregate and
241 move towards opposite poles. In many cells, anaphase accounts for a very short portion
242 of the cell cycle [30-32]. The rapidity and precise spatial control needed for a successful
243 anaphase could pose challenges for the accuracy of chromosome segregation. Here, we
244 carefully characterized the movement of chromosomes during anaphase as *Drosophila*
245 embryos proceed through the blastoderm cycles. We found that the average speed of
246 chromosome separation during these cycles is in large part controlled by the rate at
247 which nuclei complete anaphase. Spindle length and the concentration of molecular
248 motors involved in microtubule depolymerization further contribute to this process
249 ensuring a tight relationship between chromosome separation and spindle length in
250 *Drosophila* blastoderm embryos.

251

252 The mechanisms of chromosome segregation during anaphase vary across different
253 biological systems. In *Drosophila* embryos and human cell lines, chromosome to pole
254 movement (Anaphase A) dominates the total chromosome movement. On the contrary,
255 in *C. elegans* embryos, chromosome movement is almost solely achieved by pole-pole
256 separation (Anaphase B) [6]. Our analysis of microtubule dynamics and our genetic

manipulations of molecular motors argue the speed of chromosome separation is mainly set by the activity of microtubule depolymerizing motors. Notably, all three microtubule depolymerizing motors, Klp10 A, Klp67A and Klp59C contribute to setting chromosome speed in anaphase. Two major drivers of Anaphase A movement have been proposed: microtubule depolymerization at the centrosome and the kinetochore. It has been debated which of the two mechanisms contributed more. Our analysis of poleward fluxes and of mutants reducing the activity of molecular motors argues that both processes contribute to a comparable extent to Anaphase A, which might explain why it has been difficult previously to conclusively establish their relative importance. We note that the microtubule poleward flux rate we observed in this work is comparable to results in Maddox et al [16].

Our results support a model in which the rate at which anaphase is completed is a major determinant of the speed of chromosome movement. This observation can be linked to the role of molecular motors by proposing that a major function of the cell cycle oscillator is to set the activity of Klp10A, Klp67A and Klp59C and thus control the speed of Anaphase A movement. This model is supported by previous experiments showing that phosphorylation by mitotic kinases can influence the activity of MCAK, the major microtubule depolymerizing kinesin in human cells [33]. Notably, we found that the rate of anaphase completion depends similarly on the activity of mitotic kinases Polo and CycB-Cdk1 and the phosphatase PP2A. Genetic manipulations that decrease the activity of all the three enzymes result in slower progression through anaphase. Our analysis also revealed that PP2A-B55, rather than PP1, is the rate-limiting phosphatase for completion of anaphase, or at least for timing nuclear envelope reformation, consistent with previous findings [29]. These observations suggest that the rate of completion of anaphase is likely to depend on the feedback mechanisms that drive both phosphorylation and dephosphorylation of mitotic targets, as well as the feedback mechanisms by which Polo and Cdk1 control PP2A and vice versa. Understanding how these feedback mechanisms operate to control the dynamics of anaphase will reveal

286 important new insights on mitotic regulation.

287

288 Our experiments also show that cell cycle dynamics cannot fully explain the speed of
289 chromosome separation and that other molecular processes that correlate with or are
290 controlled by spindle length must be involved. A possibility is that the number of
291 molecular motors available is titrated out by the increasing number of kinetochores and
292 centrosomes associated with nuclear divisions. Consistent with this, using a Klp10A-
293 GFP transgenic line, we observed a slight decrease in the Klp10A concentration at
294 centrosomes from cycle 11 to cycle 13 (Fig S2). Alternatively, the effects of spindle
295 length on chromosome separation could arise from geometric or physical effects, for
296 example via length-dependent processes if microtubule length were to scale with
297 spindle size or other mechanisms by which forces might scale with spindle length [34].
298 These possible mechanisms are currently unclear and remain to be identified.

299

300 Scaling of spindle size with available cytoplasm has been widely reported both *in vivo*
301 and *in vitro*, and it is believed that microtubule polymerization and nucleation set
302 spindle scaling in systems of all sizes [8, 35]. In this study, we revealed an association
303 between spindle scaling and its cellular function, that is chromosome segregation.
304 Understanding if this association can be generalized to other systems, in particular to
305 other embryos undergoing reductive cleavage divisions, could reveal a conserved link
306 between these two fundamental subcellular processes. Furthermore, understanding if
307 and how the scaling identified here is influenced by the syncytial and multi-nucleated
308 nature of the cytoplasm will be important. In the future, developing an integrated model
309 that combines the dynamics of phosphorylation levels, microtubule quantity and
310 dynamics, and cell cycle progression will be essential to elucidate the mechanism of
311 scaling of chromosome speed.

312

313 **Supplemental information**

314 Figures S1-3

315 Videos S1: Nuclear division and spindle dynamics in the *Drosophila* blastoderm.

316 Video S2: Growing microtubule plus-ends labeled with EB1-GFP.

317 Video S3: Laser ablation of a mitotic spindle.

318 Video S4: Photo-conversion of kinetochore-associated microtubules.

319

320 **Acknowledgements**

321 We thank the Bloomington Drosophila Stock Center, Sharyn Endow, David Glover,
322 Michael Goldberg and Pavel Tomancak for providing stocks. We thank Mary Elting,
323 Sharyn Endow, Christine Field and Tim Mitchison for discussions. We thank members
324 of the Di Talia lab for discussions. This work was supported by NIH R01-GM122936
325 and R35-GM153490. M.R. acknowledges funding from the Human Frontier of Science
326 (Postdoctoral cross disciplinary fellowship LT000920/2020-C) and the European
327 Molecular Biology Organization (Postdoctoral fellowship EMBO ALTF 597-2021).
328 J.B., M.R., and A.K. acknowledge support from the Deutsche Forschungsgemeinschaft
329 (DFG, German Research Foundation) under Germany's Excellence Strategy – EXC-
330 2068– 390729961- Cluster of Excellence Physics of Life of TU Dresden.

331 **Author contribution**

332 Conceptualization, Y.X. and S.D.; Methodology, Y.X., J.B. and S.D.; Software, Y.X.;
333 Formal Analysis, Y.X. and S.D.; Investigation, Y.X., A.C., M.R. and A.K.; Writing,
334 Y.X. and S.D.; Visualization, Y.X. and S.D.; Supervision, S.D. and J.B., Funding
335 Acquisition, S.D. and J.B.

336

337 **Declaration of interests**

338 The authors declare no competing interests.

339

340 **References**

1. Foe, V.E. and B.M. Alberts, *Studies of nuclear and cytoplasmic behaviour during the five mitotic cycles that precede gastrulation in Drosophila embryogenesis.* Journal of Cell Science, 1983. **61**(1): p. 31-70.
2. Deneke, Victoria E., et al., *Waves of Cdk1 Activity in S Phase Synchronize the Cell Cycle in Drosophila Embryos.* Developmental Cell, 2016. **38**.
3. Mooney, P., et al., *Tau‐based fluorescent protein fusions to visualize microtubules.* Cytoskeleton, 2017. **74**(6): p. 221-232.
4. Berg, S., et al., *ilastik: interactive machine learning for (bio)image analysis.* Nature Methods, 2019. **16**(12): p. 1226-1232.
5. Brust-Mascher, I., *Microtubule Flux and Sliding in Mitotic Spindles of Drosophila Embryos.* 2002. **13**(11): p. 3967-3975.
6. Roostalu, J., E. Schiebel, and A. Khmelinskii, *Cell cycle control of spindle elongation.* Cell Cycle, 2010. **9**(6): p. 1084-1090.
7. Liang, Z.-Y., M.A. Hallen, and S.A. Endow, *Mature Drosophila Meiosis I Spindles Comprise Microtubules of Mixed Polarity.* Current Biology, 2009. **19**(2): p. 163-168.
8. Rieckhoff, E.M., et al., *Spindle Scaling Is Governed by Cell Boundary Regulation of Microtubule Nucleation.* Current Biology, 2020. **30**(24): p. 4973-4983.e10.
9. Schindelin, J., et al., *Fiji: an open-source platform for biological-image analysis.* Nature Methods, 2012. **9**(7): p. 676-682.
10. Ershov, D., et al., *TrackMate 7: integrating state-of-the-art segmentation algorithms into tracking pipelines.* Nature Methods, 2022. **19**(7): p. 829-832.
11. Lacroix, B., et al., *Microtubule Dynamics Scale with Cell Size to Set Spindle Length and Assembly Timing.* Developmental Cell, 2018. **45**(4): p. 496-511.e6.
12. Steinmeyer, J.D., et al., *Construction of a femtosecond laser microsurgery system.* Nature Protocols, 2010. **5**(3): p. 395-407.
13. Decker, F. and J. Brugués, *Chapter 5 - Dissecting microtubule structures by laser ablation*, in *Methods in Cell Biology*, E.K. Paluch, Editor. 2015, Academic Press. p. 61-75.
14. Desai, A., et al., *Anaphase A Chromosome Movement and Poleward Spindle Microtubule Flux Occur At Similar Rates in Xenopus Extract Spindles.* The Journal of Cell Biology, 1998. **141**(3): p. 703-713.
15. Mitchison, T.J., *Polewards microtubule flux in the mitotic spindle: evidence from photoactivation of fluorescence.* Journal of Cell Biology, 1989. **109**(2): p. 637-652.
16. Maddox, P., et al., *Poleward Microtubule Flux Is a Major Component of Spindle Dynamics and Anaphase A in Mitotic Drosophila Embryos.* Current Biology, 2002. **12**(19): p. 1670-1674.
17. Gandhi, R., et al., *The Drosophila Kinesin-like Protein KLP67A Is Essential for Mitotic and Male Meiotic Spindle Assembly.* Molecular Biology of the Cell, 2004. **15**(1): p. 121-131.
18. Sharp, D.J., V. Mennella, and D.W. Buster, *KLP10A and KLP59C: The Dynamic Duo of Microtubule Depolymerization.* Cell Cycle, 2005. **4**(11): p. 1482-1485.
19. Lu, W., et al., *Initial Neurite Outgrowth in Drosophila Neurons Is Driven by Kinesin-Powered Microtubule Sliding.* Current Biology, 2013. **23**(11): p. 1018-1023.
20. Girão, H. and H. Maiato, *Measurement of Microtubule Half-Life and Poleward Flux in the Mitotic Spindle by Photoactivation of Fluorescent Tubulin*. 2020, Springer US. p. 235-246.
21. Hur, W., et al., *Scale-independent topological interactions drive the first fate decision in the*

Drosophila embryo. bioRxiv, 2023: p. 2023.10.11.561879.

22. Serpico, A.F., et al., *Compartmentalized control of Cdk1 drives mitotic spindle assembly.* Cell Reports, 2022. **38**(4): p. 110305.
23. Sunkel, C.E. and D.M. Glover, *Polo, a mitotic mutant of Drosophila displaying abnormal spindle poles.* Journal of Cell Science, 1988. **89**(1): p. 25-38.
24. Glover, D.M., *Polo kinase and progression through M phase in Drosophila: a perspective from the spindle poles.* Oncogene, 2005. **24**(2): p. 230-237.
25. Conde, C., et al., *Drosophila Polo regulates the spindle assembly checkpoint through Mps1-dependent BubR1 phosphorylation.* The EMBO Journal, 2013. **32**(12): p. 1761-1777.
26. Nasa, I. and A.N. Kettenbach, *Coordination of Protein Kinase and Phosphoprotein Phosphatase Activities in Mitosis.* Frontiers in Cell and Developmental Biology, 2018. **6**.
27. Kataria, M. and H. Yamano, *Interplay between Phosphatases and the Anaphase-Promoting Complex/Cyclosome in Mitosis.* Cells, 2019. **8**(8): p. 814.
28. Haraguchi, T. and Y. Hiraoka, *Breakdown and Reformation of the Nuclear Envelope*, in *Nuclear Dynamics: Molecular Biology and Visualization of the Nucleus*, K. Nagata and K. Takeyasu, Editors. 2007, Springer Japan: Tokyo. p. 89-106.
29. Mehsen, H., et al., *PP2A-B55 promotes nuclear envelope reformation after mitosis in Drosophila.* Journal of Cell Biology, 2018. **217**(12): p. 4106-4123.
30. Brown, R., *The Effects of Temperature on the Durations of the Different Stages of Cell Division in the Root-tip.* Journal of Experimental Botany, 1951. **2**(1): p. 96-110.
31. Heath, I.B. and K. Rethoret, *Temporal analysis of the nuclear cycle by serial section electron microscopy of the fungus, Saprolegnia ferax.* Eur J Cell Biol, 1980. **21**(2): p. 208-13.
32. el-Alfy, M. and C.P. Leblond, *Long duration of mitosis and consequences for the cell cycle concept, as seen in the isthmal cells of the mouse pyloric antrum. II. Duration of mitotic phases and cycle stages, and their relation to one another.* Cell Tissue Kinet, 1987. **20**(2): p. 215-26.
33. McHugh, T., et al., *The depolymerase activity of MCAK shows a graded response to Aurora B kinase phosphorylation through allosteric regulation.* Journal of Cell Science, 2019. **132**(4): p. jcs228353.
34. Nicklas, R.B., *Chromosome Velocity during Mitosis as a Function of Chromosome Size and Position.* J Cell Biol, 1965. **25**(1): p. SUPPL:119-35.
35. Wilbur, J.D. and R. Heald, *Mitotic spindle scaling during Xenopus development by kif2a and importin α.* eLife, 2013. **2**: p. e00290.

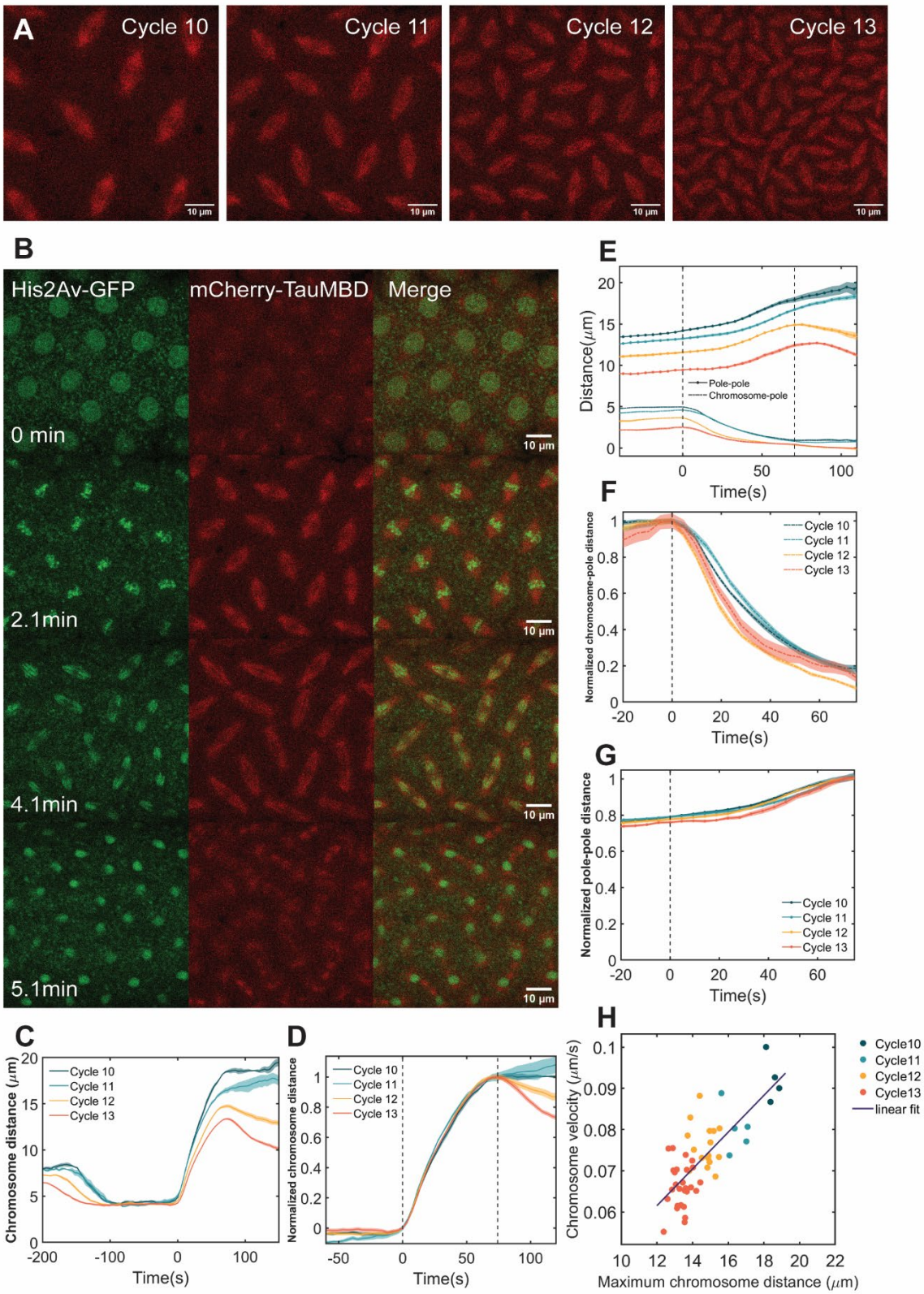

Figure 1. Chromosome velocity during anaphase scales with spindle length.

Figure 1. Chromosome velocity during anaphase scales with spindle length. (A) Mitotic spindles in the *Drosophila* embryo from syncytial cycle 10 to 13, labeled with mCherry-Tau microtubule binding domain. (B) Chromosome and microtubule dynamics during mitosis at cycle 11. From top to bottom: prophase, metaphase, anaphase, telophase. (C) Distance between the leading edges of sister chromosomes during anaphase as a function of time. (D) Normalized chromosome distance from (C) by the maximum distance. Left dotted line: anaphase onset. Right dotted line: end of chromosome movement during anaphase, when chromosome distance reached its maximum or plateau. (E) Pole-to-pole distance and chromosome-to-pole distance during anaphase from cycle 10 to13. (F and G) Both chromosome-to-pole distance and pole-to-pole distance could be rescaled across cycles. (H) The average chromosome velocity during anaphase scales with the maximum chromosome distance, which serves as a proxy of spindle length.

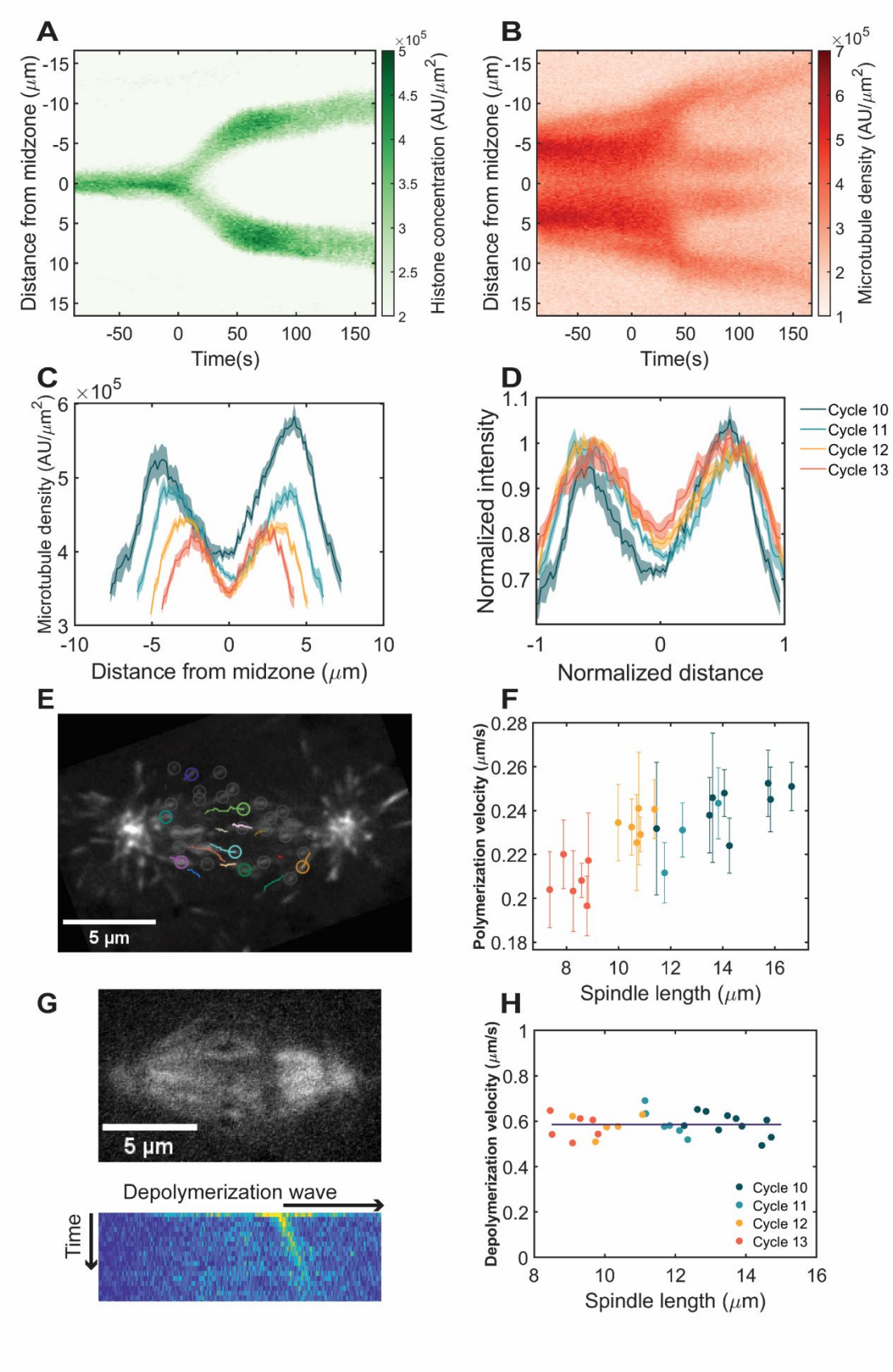

Figure 2. Microtubule dynamics contribute to spindle scaling in the *Drosophila* embryo.

Figure 2. Microtubule dynamics contribute to spindle scaling in the *Drosophila* embryo. (A and B) Kymograph of chromosome separation (A) and spindle dynamics (B) in a cycle 10 embryo, labeled with His2Av-GFP and mCherry-Tau microtubule binding domain. T = 0 indicates anaphase onset. (C) Line scans of microtubule density along the spindle long axis during metaphase. (D) Rescaled microtubule density from cycle 10 to 13. (E) Microtubule plus end tracking with EB1-GFP in a cycle 12 embryo. (F) Microtubule polymerization velocity as a function of spindle length. Each data point represents the mean velocity ± SEM of all tracked comets in one spindle. (G) Laser ablation of microtubules in a cycle 11 embryo, labeled with Jupiter-GFP. A wave of depolymerization was visualized after projecting the differential intensity onto the spindle long axis. (H) Microtubule depolymerization velocity as a function of spindle length.

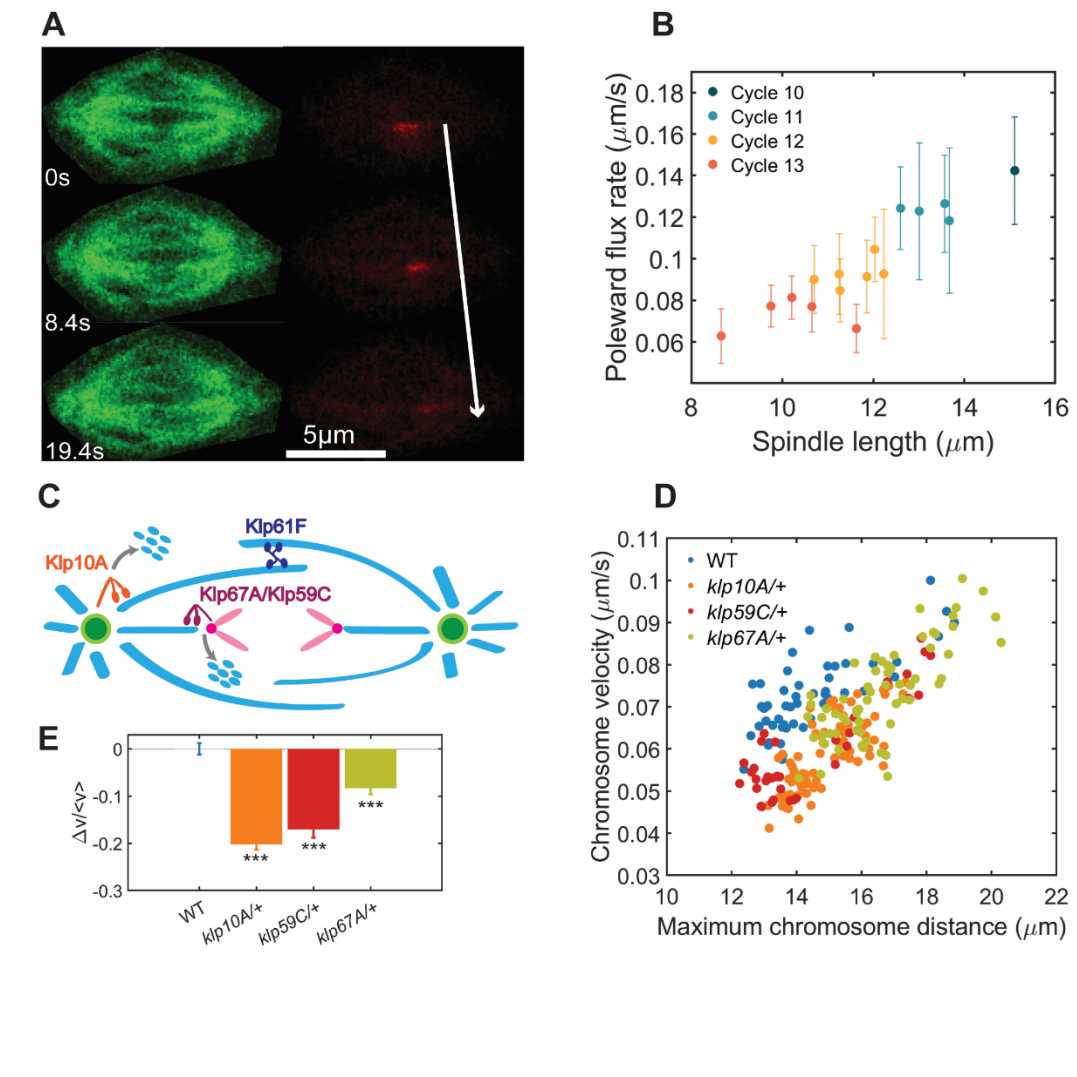

Figure 3. Microtubule-depolymerizing motors regulate chromosome velocity.

Figure 3. Microtubule-depolymerizing motors regulate chromosome velocity. (A) Photo-conversion of the kinetochore-associated microtubules using α-tubulin-tdEOS embryos. (B) Poleward flux rate scales with spindle length. Error bars indicate 95% confidence interval. (C) Microtubule-depolymerizing motors Klp10A, Klp59C and Klp67A contribute to chromosome-to-pole movement (Anaphase A), while microtubule-sliding motor Klp61F contributes to pole-pole separation (Anaphase B). (D) Correlation between chromosome velocity and maximum chromosome distance in heterozygous motor mutants. (E) Average relative change in chromosome velocity between wild-type and heterozygous motor mutants. Data shown as mean ± SEM (*** $P<0.001$).

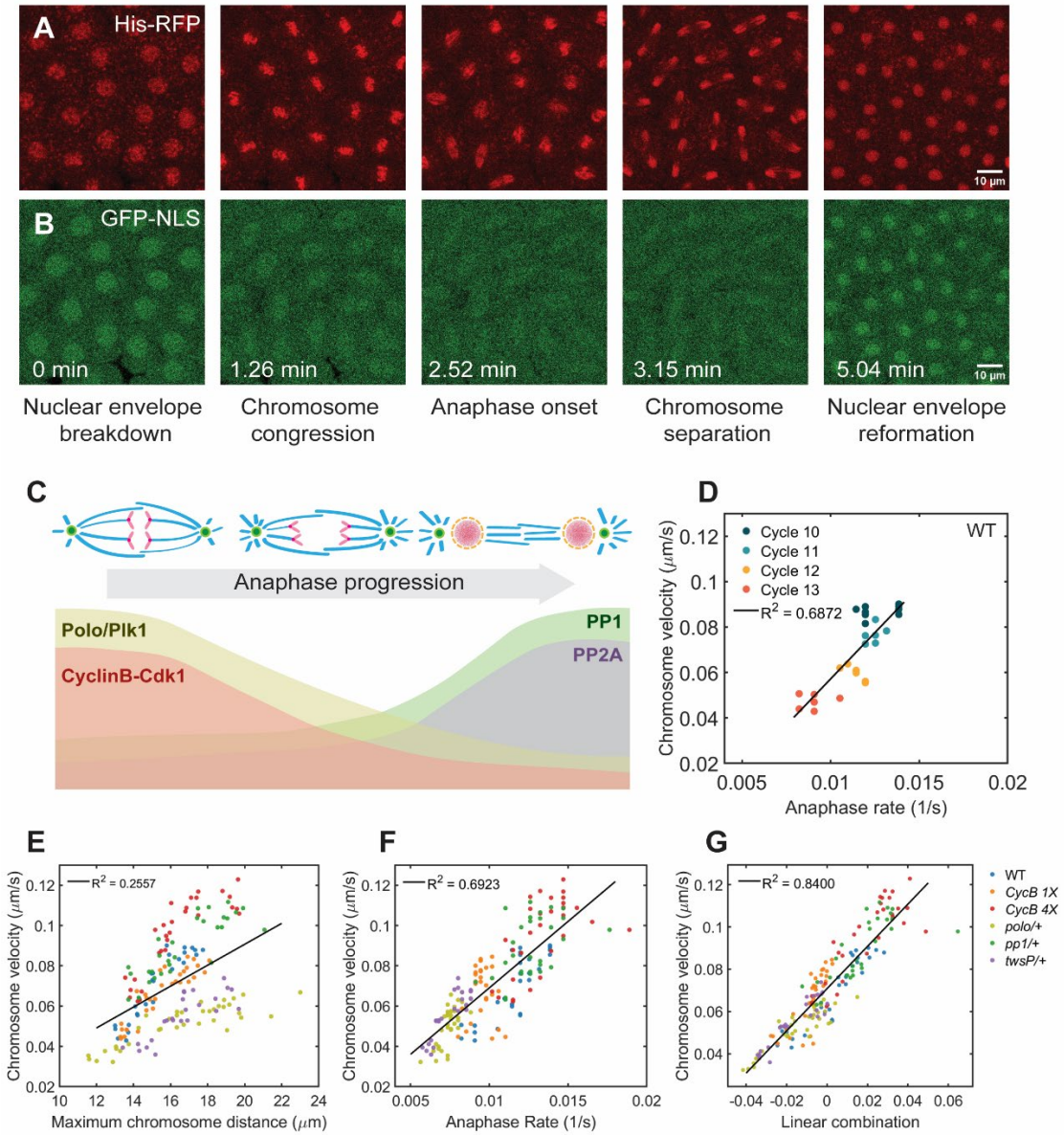

Figure 4. The cell cycle oscillator and spindle length together set the speed of chromosome movement in anaphase.

Figure 4. The cell cycle oscillator and spindle length together set the speed of chromosome movement in anaphase. (A and B) Dynamics of chromosome and nuclear localization signals (NLS) in a cycle 11 embryo, from nuclear envelope breakdown to nuclear envelope reformation. (C) Schematic of anaphase progression and the corresponding activity of mitotic kinases and phosphatases. (D) Chromosome velocity scales with anaphase rate in a wild-type embryo. (E) Chromosome velocity as a function of maximum chromosome distance in heterozygous cell cycle mutants. (F) Chromosome velocity as a function of anaphase rate in heterozygous cell cycle mutants. (G) Chromosome velocity scales with a linear combination of anaphase rate (70%) and spindle length (30%).

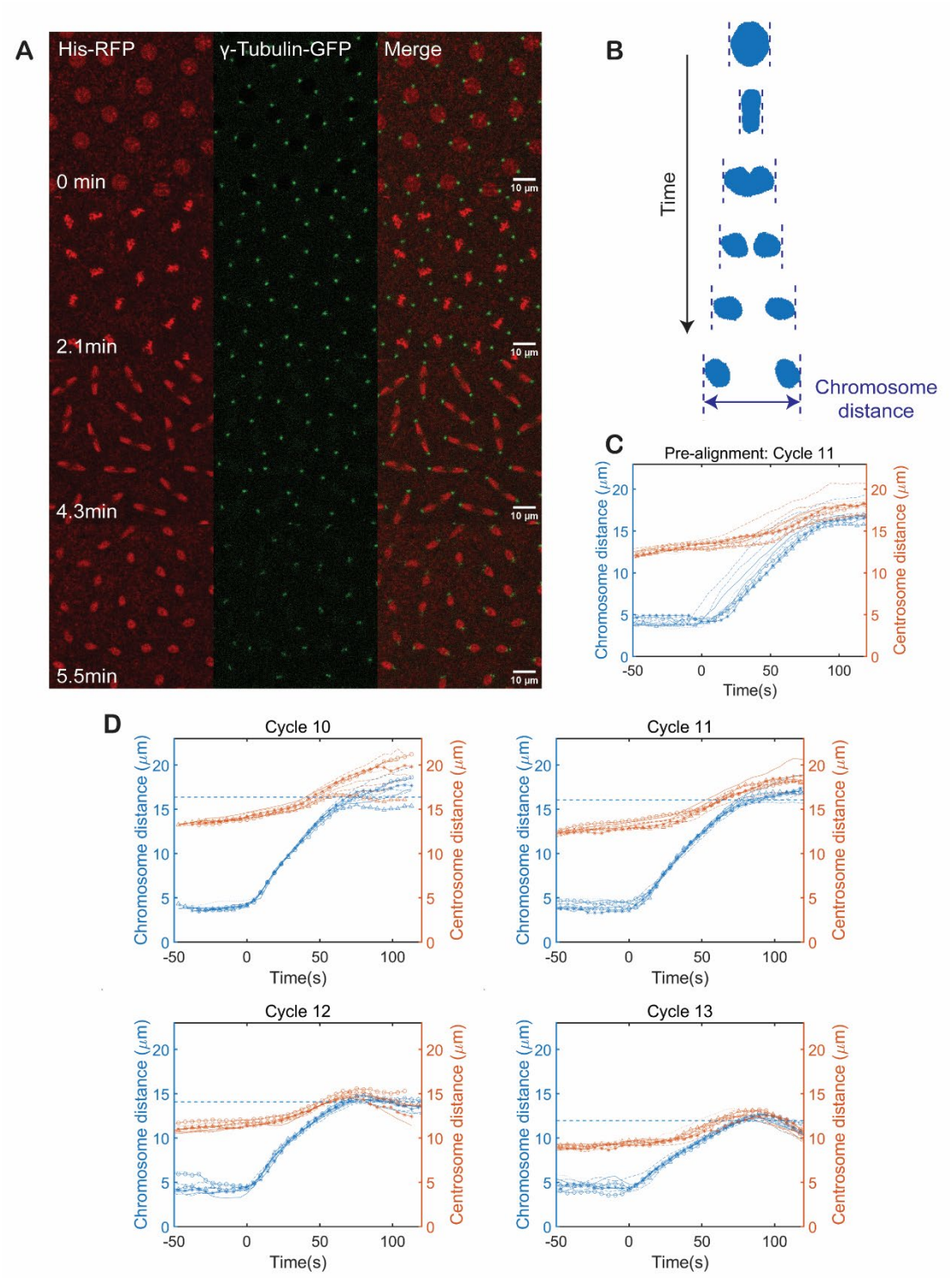

Figure S1. Quantification of chromosome distance, pole-pole distance and approximation of anaphase spindle length. (A) Chromosome movement and centrosome dynamics during mitosis at cycle 11. From top to bottom: prophase, metaphase, anaphase, telophase. Chromosomes are labeled with His-RFP, centrosomes are labeled with γ-Tubulin-GFP. (B) Method for quantifying chromosome distance.

Blue masks represent chromosome segmentations. Dashed blue lines indicate the leading edges of chromosomes during separation. (C) Chromosome distance and centrosome distance as a function of time at cycle 11, individual nuclear division events were represented with the same linestyle. A slight asynchrony of chromosome movmement was observed. (D) Aligned chromosome distance and centrosome distance as a function of time from cycle 10 to 13. Chromosome movements were shifted in time to collapase the curve of chromosome distance. T = 0 indicates anaphase onset. Dashed blue line indicates the average of maximum chromosome distance, which serves as a proxy for spindle length in anaphase.

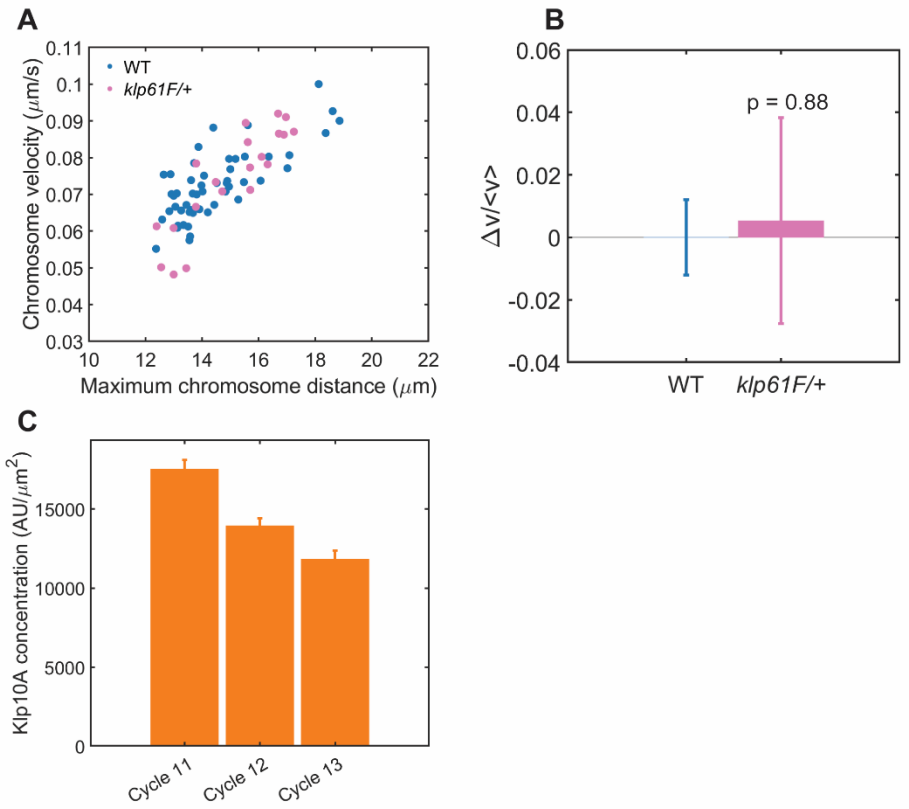

Figure S2. Unlike the microtubule depolymerizing motors, microtubule sliding motor Klp61F (Kinesin-5) does not regulate chromsome velocity. (A) Correlation of chromosome velocity and maximum chromosome distance in wild-type and *klp61F* heterozygous muants. (B) Average relative change in chromosome velocity between wild-type and *klp61F* heterozygous mutants. (C) Klp10A concentration at centrosomes is titrated as the cell cycles progress. Data shown as mean ± SEM.

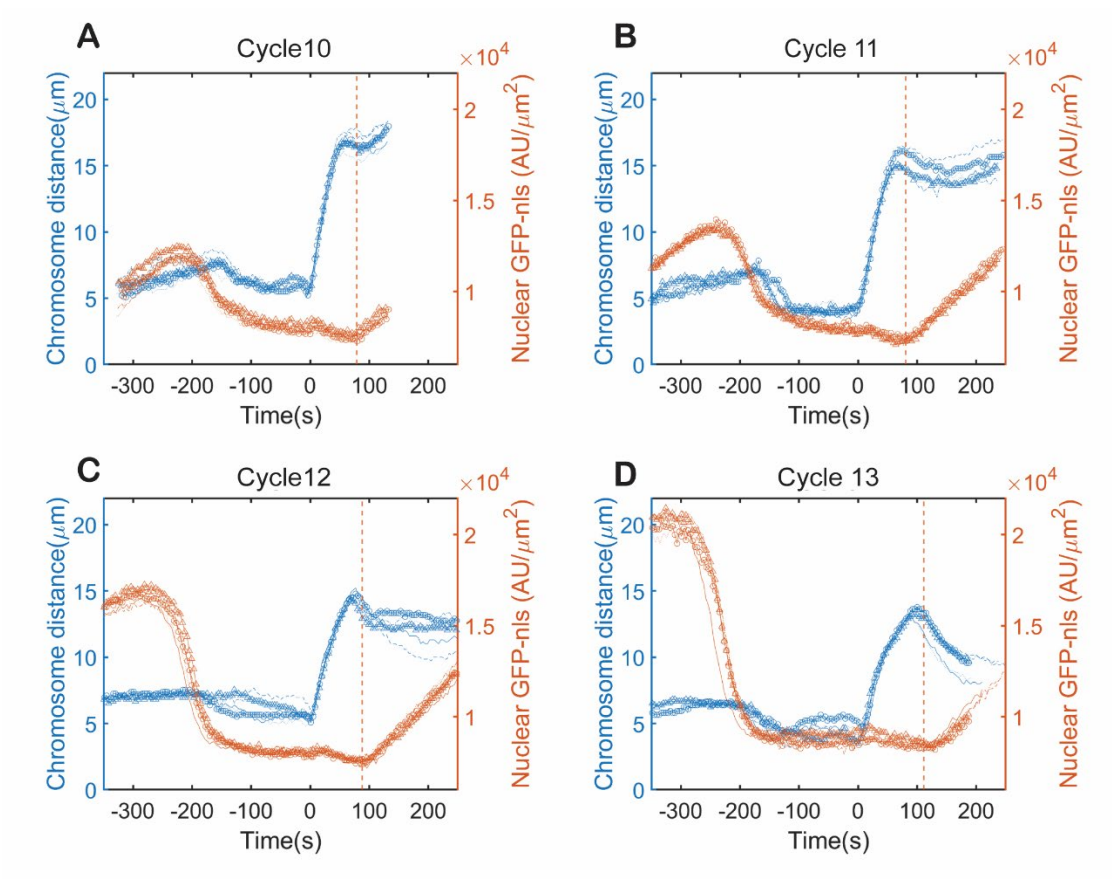

Figure S3. Anaphase duration lengthens as the cell cycles progress. (A-D) Chromosome distance and nuclear localizing GFP concentration as a function of time. T = 0 indicates anaphase onset, dashed orange line indicates the average time point of nuclear envelop reformation.

418 **EXPERIMENTAL MODEL AND STUDY PARTICIPANT DETAILS**

419 **Fly lines and husbandry**

420 Klp10A P mutant flies were raised at room temperature (~21ºC) on glucose food
421 (Archon, Cat #D210). All other flies were raised at room temperature on standard
422 molasses food (Archon, Cat #B20101).

423

424 **METHOD DETAILS**

425 **Embryo collection and processing**

426 Before imaging, adult flies with genotypes of interest were housed in a cage covering
427 an apple juice plate at 25ºC, supplemented with yeast paste. Embryos were collected
428 over 2 hours on a fresh plate, dechorionated with 50% bleach for 1 minute, and mounted
429 in Halocarbon oil 27 on a gas-permeable membrane with coverslips.

430 **Microscopy**

431 Embryos were imaged on a Leica SP8 laser scanning confocal microscope equipped
432 with a Leica 20x oil-immersion objective 0.75NA (HC PL APO CS2 20x/0.75 IMM)
433 unless otherwise noted.

434 **Microtubule plus end imaging**

435 Embryos were imaged with a spinning disk confocal microscope (IX83 Olympus
436 microscope with CSU-X1 Yokogawa disk) connected with two iXon DU-897 back-
437 illuminated EMCCD camera (Andor). Experiments were acquired using an Olympus
438 100x silicon oil objective1.35 NA and imaged at 1-2 frames per second.

439 **Laser ablation experiments**

440 With the Jupiter-GFP line, metaphase spindles were imaged using a spinning disk
441 confocal microscope (Nikon Ti Eclipse, Yokogawa CSU-X1) equipped with an
442 EMCCD camera (iXon DU-888 or DU-897, Andor) and a 100x oil-immersion objective.
443 Images were acquired with the Andor iQ software. Laser ablation was performed
444 according to Rieckhoff et al on a custom-built femtosecond laser microsurgery system.
445 Briefly, line cuts parallel to the spindle equator were induced by moving the sample
446 with a high-precision piezo stage (PInano) relative to the stationary cutting laser. The

447 ablation was controlled by a custom-written software managing the piezo-stage and a
448 mechanical shutter in the optical path. Each embryo was cut only once and imaged at
449 intervals of 200-300ms/frame.

450 **Photo-conversion experiments**

451 Photo-conversion experiments were performed on the Leica SP8 microscope with the
452 FRAP Module in the Leica Application Suite X (LAS X). Experiments were acquired
453 using a Leica 63x oil objective 1.40 NA (HC PL APO CS2 63x/1.40 OIL). Spindle
454 microtubules were excited with 0.1% 405nm laser for 1 millisecond to induce photo-
455 conversion from GFP to RFP.

456

457 **QUANTIFICATION AND STATISTICAL ANALYSIS**

458 **Chromosome segmentation and tracking**

459 Movies of the histone channel were loaded in ilastik for chromosome segmentation
460 using the pixel classification workflow. Pixels were manually annotated as either
461 chromosome or cytosol to train the classifier. Training was considered complete when
462 the live output aligned with visual judgement. A prediction map for chromosome
463 segmentation was generated. The raw movie and prediction map were reloaded into
464 ilastik for the tracking or manual tracking workflow, with the division events manually
465 labeled. For automatic tracking, the correctness of the tracking was manually verified
466 before further quantification. Either the maximum number of trackable nuclear division
467 events in frame or at least five divisions were recorded for each cycle.

468 **Quantification of chromosome distance and chromosome velocity**

469 For segmented chromosome undergoing mitosis, a bounding box was drawn
470 surrounding a single nucleus or sister chromosomes. The length of the bounding box
471 along the division axis was quantified as chromosome distance in real-time. Anaphase
472 onset was determined as the first frame when chromosome distance started to increase
473 after metaphase. The total chromosome movement during anaphase was quantified
474 from anaphase onset till the chromosome distance plateaued (e.g. in cycles 10 and 11)
475 or reached maximum before recoil (e.g. in cycles 12 and 13). Average chromosome

476 velocity was calculated as total chromosome movement divided by the duration of the
477 movement. To compare the velocity among genotypes controlling for spindle length,
478 data points were divided into 4 bins based on spindle lengths (ranging from 12 μm to
479 20 μm). The average chromosome velocity of the wild-type in these bins was quantified
480 as a refence velocity $<v_{WT}>$. For each bin, the relative change in velocity was quantified
481 as $(v_{mutant}-<v_{WT}>)/<v_{WT}>$. Relative changes in all bins were summarized for each
482 genotype.

483 **Quantification of Anaphase A and B movement**

484 Using the TrackMate plugin in FIJI, centrosomes marked with γTubulin were detected
485 with the LoG detector and tracked with the LAP tracker, allowing for splitting.
486 Centrosome tracks were manually curated and matched with the corresponding
487 chromosome tracks. Anaphase B movement was quantified by measuring the separation
488 of two centrosomes at opposite spindle poles. Anaphase A movement was calculated by
489 subtracting Anaphase B movement from the total chromosome movement.

490 **Quantification of microtubule density**

491 For spindles at metaphase, a line of defined thickness (2μm) along the spindle long axis
492 was used to measure fluorescence intensity and calculate the density profile.

493 **Quantification of microtubule polymerization velocity**

494 EB1 comets in the spindle region were tracked with the TrackMate plugin in the FIJI
495 software, applying the LoG detector and simple LAP tracker. Tracks were filtered by
496 duration (~ 3-15s) and linearity (> ~ 0.9) and then manually screened. The speeds of all
497 correctly tracked comets within each spindle were averaged to represent the
498 microtubule polymerization velocity for that spindle.

499 **Quantification of microtubule depolymerization velocity**

500 The amount of depolymerized microtubule during a time interval was calculated by
501 subtracting raw images with a time difference of 0.4~0.6s from each other and
502 integrating these differential intensities perpendicular to the spindle long axis.
503 Depending on the position of the cut, the integrated differential intensities along the
504 spindle long axis showed one or two well-defined peaks. The peaks moved toward the

505 nearest pole following ablation. The more prominent peak was fit to a Gaussian
506 function to quantify the position of the maximum. The position of the maxima over
507 time was fit to a line to determine the microtubule depolymerization velocity.

508 **Quantification of poleward flux rate**

509 To analyze the poleward flux, for images in the photo-converted channel, we computed
510 the average fluorescence intensity along the spindle length and evaluated the points
511 where this quantity crosses a value close to half-max, estimated as half of the 95
512 percentile of fluorescence intensity values. These points defined the ends of the photo-
513 converted region. For instances when the spindles remain a constant length and where
514 microtubules on both sides of the mid-spindle were properly labeled, the speed of
515 poleward flux was estimated as half of the speed at which the two ends moved apart.
516 For instances where microtubules were labeled only on one side of the spindle, we
517 computed the speed as the distance between the photo-converted end and the closest
518 centrosome. The positions of centrosomes were estimated by computing the initial and
519 final positions where intensity in the green (non-converted) channel crossed a value
520 close to half-max (half of the 95 percentile of fluorescence intensity values).

521 **Quantification of nuclear envelope reformation**

522 The Histone-RFP channel in the time-lapse movie was used to segment nuclei and track
523 nuclear division with ilastik. The nuclear concentration of GFP-NLS signal, together
524 with chromosome distance, was plotted as a function of time. The onset of nuclear
525 envelope reformation was inferred from the time point when the GFP-NLS
526 concentration began to increase after chromosome separation.